Research Article

Ferromagnetic topological crystalline insulating phase in the π-stacked graphene nanobelts under a small pressure

Małgorzata Wierzbowska[1]

Abstract
This work presents a topological material based on the graphene nanobelts. It is intrinsically magnetic. The band inversion in this system is partial and anomalous, as it was recently found in the Au-doped graphene and 2D molecular crystal. The metallic edge states with the Chern number equal to 1 exist in the ferro- and antiferromagnetic phase. The edge states become gapless at a small pressure, around 0.87 GPa, applied along the stacking axis. Their dispersions are not symmetric for the spin up and down. The graphene nanobelts are π-stacked with the AB-type, and the zigzag edges are terminated with the O and H atoms at the opposite sides, in the reversed order along the stacking axis. The propagation of the topological edge states is parallel to the O···H-interaction direction, across the stacked belts.

Keywords Topological insulators · Ferromagnetic materials · Graphene nanobelts

PACS No. 73.00.00 · 73.20.–r · 73.20.At · 75.25.+z · 75.70.Cn · 75.70.Rf

1 Introduction

Graphene has shown many appealing properties, since its discovery in 2004 and the Nobel Prize for Novoselov and Geim in 2010 [1, 2]. Due to the existence of the Dirac-cone states, the topological insulating (TI) phase has been searched there. However, without success, because the spin-orbit coupling (SOC) in this material is negligible. On the other hand, a light doping of graphene with the hydrogen atoms strengthens the SOC by four orders of magnitude [3, 4]. Recently, the status of the search for the TI phase in graphene has changed with a prediction of the TCI phase in the twisted graphene bilayers [5] with the negligible SOC effects, both the intrinsic and Rashba type. The SOC-free TCI phase was found also at the domain-wall of the AB- and BA-stacked graphene bilayers [6–8] and in the 2D molecular crystal [9].

Here, the TCI phase is found in the π-stacked magnetic graphene nanoribbons at a small pressure of about 0.87 GPa, at which the metallic edge states become gapless. The belts are π-stacked in the AB-type order, the same as in graphite. The zigzag edges are terminated with the oxygen and hydrogen atoms on the opposite sides, with an alternation of the O and H atoms in the π-stacking direction—here called the AB-reversed order. It is plausible, that the vertical O···H-interactions play a role in the formation of the topological states, where the mechanism would be the same as in the stacked 2D molecular system [9].

The band inversion is essential for the topological phase, but not sufficient. In the conventional TIs, the time-reversal properties are responsible for the BI [10]. In contrast, the TCIs are ruled by the crystalline symmetry, the SOC should be in principle absent there [11, 12]. These

Electronic supplementary material The online version of this article (https://doi.org/10.1007/s42452-019-0723-x) contains supplementary material, which is available to authorized users.

✉ Małgorzata Wierzbowska, wierzbowska@unipress.waw.pl | [1]Institute of High Pressure Physics, Polish Academy of Sciences, Sokołowska 29/37, 01-142 Warsaw, Poland.

SN Applied Sciences (2019) 1:748 | https://doi.org/10.1007/s42452-019-0723-x

Received: 9 November 2018 / Accepted: 4 June 2019 / Published online: 19 June 2019

materials are supposed to be built of the light elements only [11]. Very recently, the new type of the BI—namely the anomalous BI—was reported in graphene with the substitutional N_3-centers additionally doped with the Au atoms [13]. The anomalous character of the BI in the above system shows up as the inversion which occurs between the conduction band minimum (CBM) and the bands laying deeper below the valence band top (VBT). Our previous work, on the other hand, reports the partial BI in the 2D molecular crystal [9]. It will be demonstrated in this work, that a combination of both types of the BI, the partial and anomalous between the VBT and the bands laying above the CBM, occurs in the π-stacked graphene nanobelts.

The magnetism in the graphene nanobelts originates from the edge termination. It is known for a few years that a saturation of the zigzag edges with the double and single bonds on the opposite sides leads to the formation of the magnetic moments at the edges [14, 15]. We proposed to use this effect in the random-access memory devices [16]. Here, the saturation of the zigzag edges with O and H is responsible for two effects: magnetism and the topological phase. The second phenomenon occurs when the interlayer distance is slightly decreased. We think that these systems are possible to synthesize, since the chemical manipulation at graphene edge is nowadays an easy task [17].

To date, a very few TIs among native magnetic materials, such as undoped crystals, are known. One of them is the antiferromagnetic Heusler compound [18]. Usually, the conventional TIs are doped with magnetic elements. Some examples of the transition metals are V, Cr, Mn, Fe and Co in chalcogenides [19–28]. It is desired to know whether and how the doping might change the topological states. It was believed that the nonmagnetic doping does not influence the topological properties [29]. In contrast, the effect of magnetic impurities and magnetic field opens the gap at the Dirac cone of the surface states in some 3D TIs [21–23], challenging the robustness of the topological phase. While some other TIs with the nonmagnetic dopants pass the above test [24–26]. Recently, it has been shown that the nonmagnetic impurities such as indium in Bi_2Se_3 also open the surface band gaps [28], in contrast to previous belief [29]. Thus, a discussion on a role of the magnetic anisotropy of the add atoms at the surface and in the bulk, and the position of the impurity band, for a protection of the topological surface states, is still actual [19, 27]. Moreover, the topological properties are correlated with the mechanisms of the long-range magnetic order, and this fact influences the Curie temperature [20, 27]. Since the impurities might harm the topological properties, and the spin-polarized states at the surfaces usually do not coexist with the bulk magnetism, a generation of the spin-polarized current through the bulk of the TI was proposed [30].

In view of the controversy on the topological protection and doping, and in contrast with the doped TIs, the intrinsically magnetic and SOC-free system with the asymmetric metallic surface states are presented. These states become gapless under a small pressure applied along the stacking axis. In the infinite 2D system, the band gap lies above the two bands above the Fermi level. In the terminated system, the magnetic edge states could be accessed with the electron excitation via the absorption of light. The proposed systems pave the way for a design of naturally magnetic TCIs based on graphene and the hydrogen interactions. In the antiferromagnetic (AF) phase, this system is similar to the 3D TCIs composed of the AF stacks of the 2D layers, predicted by the symmetry considerations [31, 32]. However, with the difference that the dimensions of the systems presented here are lower. The ferromagnetic (FM) TCIs, on the other hand, were to date only predicted in the spinel structure materials belonging to the class of the filling-enforced semimetals [33].

2 Results

2.1 The atomic, electronic, and magnetic structure

The atomic structure and the symmetry of the proposed system are presented in Fig. 1a–c. The side and top views at the AB-stacked graphene nanobelts with the alternated (named reversed) O and H terminations are drawn in Fig. 1a, b, respectively. This 2D nanomaterial contains two π-stacked armchair ribbons in the elementary cell, and transforms with the inversion operation, as shown in Fig. 1c. The optimized separations between the belts do not differ much for the FM and AF phases and equal to 3.439 Åand 3.437 Å, respectively.

Let us further investigate the symmetry of these systems. The magnetic symmetry groups (MSG) are of the types I-IV, where the type I is equivalent to the nonmagnetic symmetry groups and can be described solely by the unitary symmetry operations. Other types, II–IV, have an equal number of the unitary and anti-unitary elements: $M = G + A$. The anti-unitary part A can be written as a product of the spacial and time-reversal operations $\tau\Theta$. If τ belongs to G, then our system is of the type II. In the opposite case (τ does not belong to G), our system is of type IV (called sometimes IIIb) when τ is a pure translation. In case τ is not a pure translation, our system is of type III (called sometimes IIIa). For a reference see for example works [32, 33]. The atoms of our elementary cell transform with the superposition of two operations: the rotation by 180° around the stacking (z-axis) and the

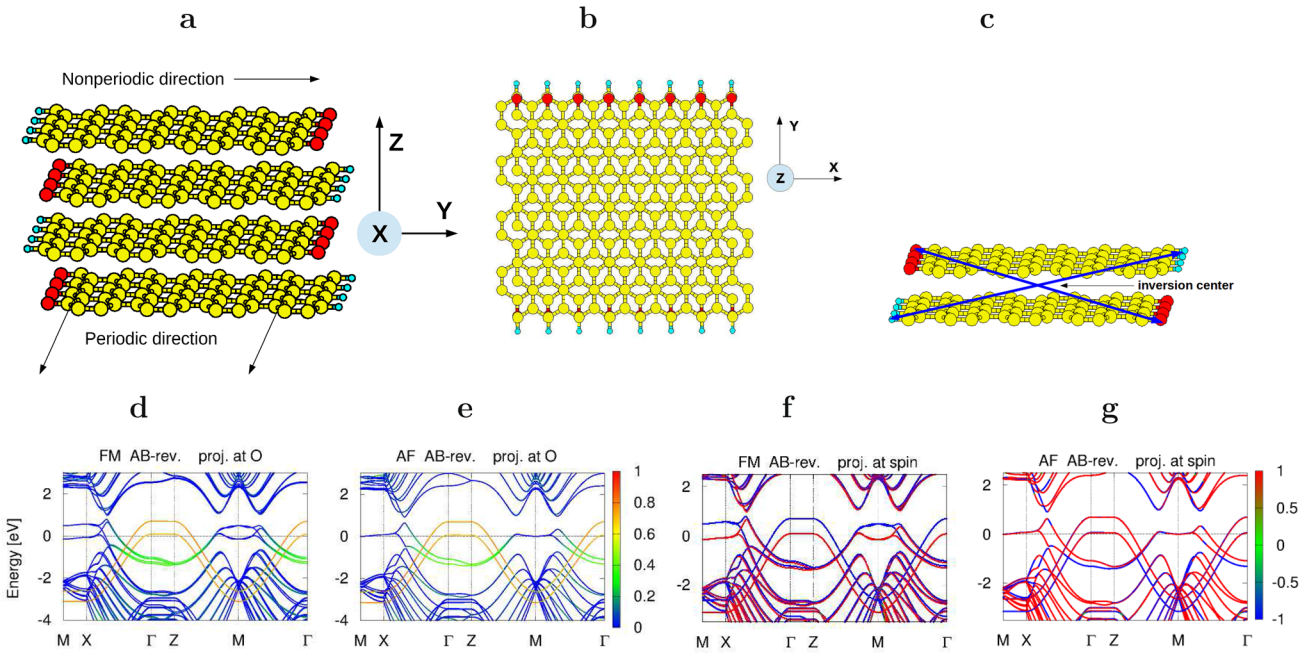

Fig. 1 The atomic structures (**a**–**c**) and the band structures (**d**–**g**) of the graphene nanobelts. The FM or AF case is denoted above each electronic structure. The projections at the oxygen-localized Wannier functions **d**, **e** are in color legends. If 100% of the band was built of the oxygen-localized functions then the band color would be red (the component factor was 1). The projection at spin-*z* component **f**, **g** is also in color legends. The absence of the green color in **f**, **g** indicates the negligible SOC

fractional translation along this axis (by $\frac{1}{2}$ of the lattice constant *c*). Equivalently, one can say that there is a glide mirror symmetry (*pmg*2). The systems studied here can be classified as 3.4 MSG IV (P_a112) [33].

The band structures, calculated with the density functional theory (DFT), with the SOC included, are presented for the FM and AF cases in Fig. 1d–g. The Fermi level, positioned at the zero energy, is around 0.7–0.9 eV below the VBT. Both magnetic phases are metallic, and they change the character to semiconducting after the *n*-type doping with one electron per each oxygen atom (two electrons per the elementary cell). The FM phase is energetically more favorable than the AF phase, by 31 meV per the elementary cell.

In Fig. 1d, e, the colors indicate a contribution of the oxygen states to the Bloch functions. The oxygen component predominates the valence band along the stacking axis, while the bands along the belt axis are rather built by carbons. The direct bandgap in the FM phase is 0.18 eV and located at the *k*-point on the line between the Γ and X symmetry points. In contrast, the band gap in the AF phase is indirect and equals to 0.2 eV. Its location is between the VBT at the Γ point and the CBM at the same k-point as in the FM phase.

The absolute magnetization, per one oxygen in the elementary cell, is 0.55 μ_B for the FM phase and 0.28 μ_B for the AF phase. The projections of the band structures onto the majority and minority spin-component are in Fig. 1f, g. The absence of the states which mix the large and small spinor components, in the whole Brillouin zone, is a signature of the SOC-free character of the band structures. The magnetic moments are mainly localized at the zigzag edges, as seen from the spin maps for the FM and AF phases in Figure S1a-j in the supporting information (SI). In the AF phase, the local spin moments sit mainly at the oxygen atoms, i.e., the magnetization is localized in the planes of the graphene belts. The local moments in the FM phase are similar to those in the AF phase when comparing the belts planes. Additionally, the FM phase possesses more rich spin structure, which is shifted away from the belts planes above and below the carbons adjacent to hydrogens, as presented in Figure S1c-d and S1e-g in SI.

Interestingly, the systems presented in this work have a very nice property which is desired for the photovoltaics. Namely, the carbon rings terminated with the atomic groups which contain the O···H or N···H-interactions possess the property of the space separation of the charge carriers [34]. In other words, the electrons and hole move along different paths through the material. Such separation reduces the unwanted charge recombination of carriers, which is one of the key factors lowering the conversion efficiency of the solar cells.

Similar property has been suggested to appear in the organic lead halide perovskites [35, 36] and covalent organic frameworks [37]. It is a nice coincidence that this effect occurs also in the O= and H– terminated graphene nanobelts. This fact is clear from Figures S2 and S3 in SI, which present the maps of the Bloch's functions at the VBT and CBM for the FM and AF phase, respectively.

2.2 The topological properties

We assume the 2D system to be finite along the belt axis (the *Y* Cartesian axis). The 2D band structures and the 1D edge states of the systems truncated along the belts (the *X* Cartesian axis) are analyzed in Fig. 2. In particular, the dispersions are drawn in Fig. 2a, b for the FM phase and in Fig. 2d, e for the AF phase. The propagation direction of the edge states is along the stacking axis (the *Z* Cartesian axis), which is also the direction of the O···H-interactions. For the FM phase, two spin-polarized and not degenerate

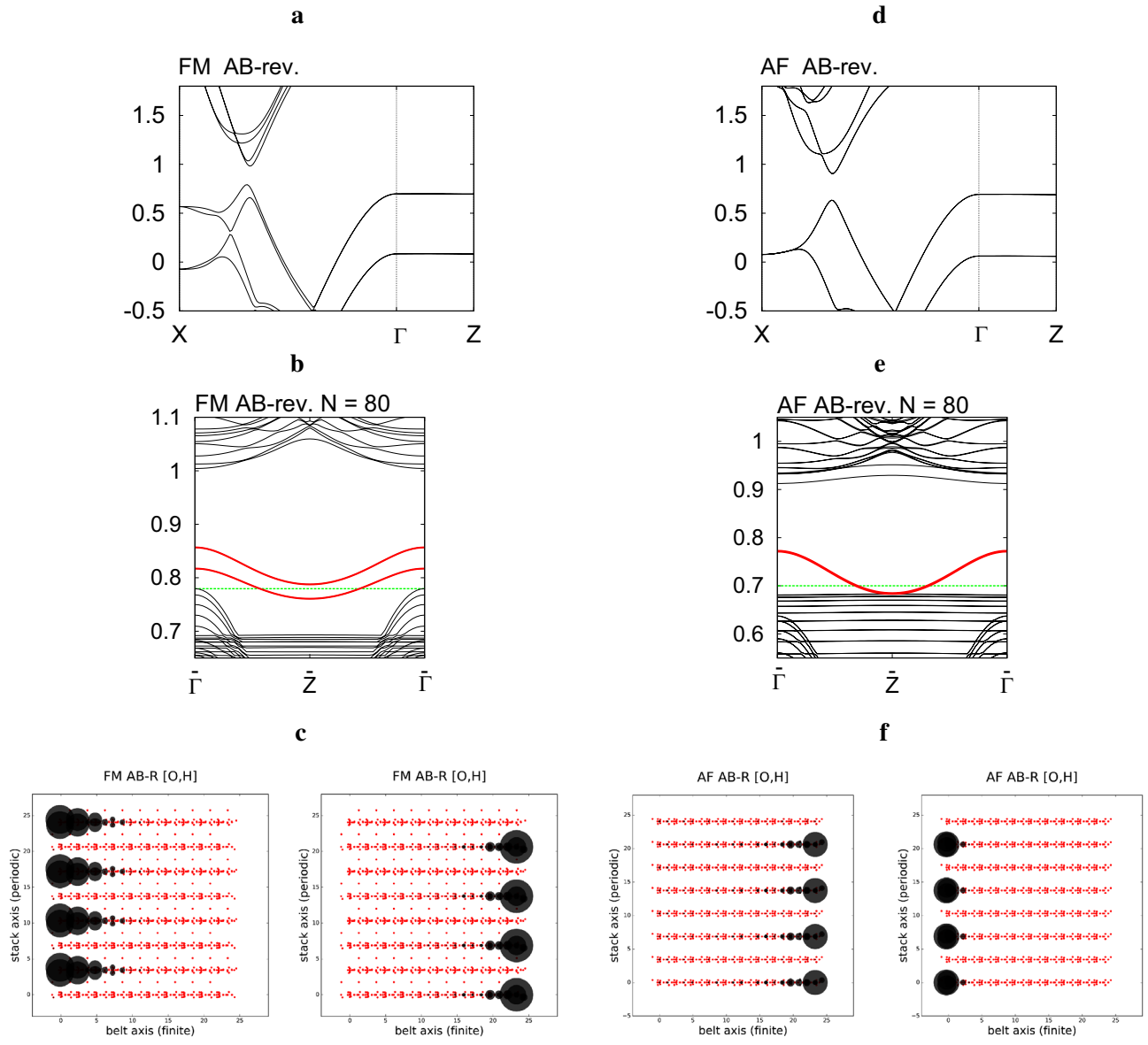

Fig. 2 The 2D band structures (**a**, **d**) and the 1D edge states (**b**, **e**) for the FM and AF phase, respectively. The VBT is marked with the green dashed line. The number of cells, *N*, in the truncated finite direction (*X*-axis) is given above the corresponding panels. The visualization of the orbitals **c**, **f** associated with the edge states which are marked in the dispersions **b**, **e** with the red lines. The red dots in **c**, **f** are the centers of the Wannier functions

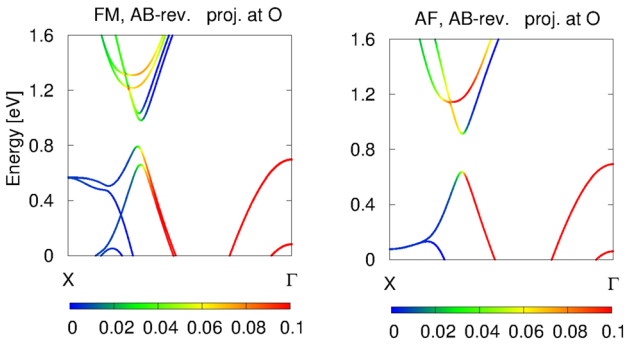

Fig. 3 The projection of the VBT and CBM of the FM and AF case at the oxygen-localized Wannier functions, with the enlarged color legend, up to 10%, for a better resolution of the weak effect

edge states, due to the nonsymmetric magnetic phase, cross the gap. In the AF phase, the state within the gap which appears to be single is in fact doubly degenerate for the two spin components. Both magnetic orders are characterized with the parabolic dispersions of the edge states, falling within the band gap of the 1D structure. This property could be one of the prerequisites of the topological crystalline insulating phase, under the condition that the edge states become gapless under a small pressure. Such effect occurs in the studied systems, as will be clear later.

Figure 2c, f displays the spacial localization of the wave functions of the two edge states, in the FM and AF phase. These states are well localized at the cut edges of the belts. In the AF case, both edge states localize at the two ends of the same belt. This is, in fact, every second belt of the stack, because two belts are in the elementary cell. In the FM case, the edge states on the left- and right-hand side of the belt localize at the alternating belts of the stack. Moreover, the wave function of the edge state which is more occupied by the electrons is less localized. It extends more to the interior of the belt, in comparison with the less occupied edge state (the one which is higher in the energy).

Let us switch to the band inversion. It is almost absent for both magnetic phases, if one looks only at Fig. 1d–g. However, an enlargement of the color scale reveals more subtle effects. The detailed characteristics is presented in Fig. 3. The contribution of the oxygen-localized states to the Bloch functions, which is printed up to 10%, shows a signature of the band inversion. The two bands of the CBM are composed of the O-states in much smaller part than the VBT states. The two states just above the CBM contain much more substantial portion of the oxygen states. This type of the BI is similar to the earlier published two cases: The first type of the BI, called anomalous, was reported for the Au-doped N_3-centers in graphene, where the CBM exchanged its character with the bands laying deeper below the VBT [13]. The second type of the BI, called partial, was reported by us for the 2D molecular crystal, where the bands inversion was mixed with the non-inversed components [9]. It is worth to notice that these types of BI are numerically observed in the three reported cases which are the π-stacked systems.

The maps of the square-root function of the Bloch densities—equivalent to the absolute values of the Bloch functions—are presented in Figures S2 and S3 in SI for the FM and AF phases, respectively. The VBT Blochs are mainly composed of the states which are localized within the planes of the belts, close to the O= terminated edge. In contrast, the CBM Bloch functions are composed of all carbon states which are distant from the belt edges, and the maxima of these states are shifted a bit away from the belt's plane. This shift is a signature of the p_z-orbital character of the CBM.

Since our systems are magnetic, there is a question on the proper topological invariant, i.e., whether one could apply the Z_2 invariant [38]. In fact, the band gaps are positioned above the Fermi levels of the magnetic phases. One needs to occupy two more bands in order to move the Fermi level inside the band gap. However, if all states up to this gap are occupied, the magnetism will vanish. The only way to access the magnetic topological edge states would be the excitation of electrons via the absorption of a photon. Therefore, when analyzing the symmetry of the entangled valence band manifold, these unoccupied two states must be included. This way, we arrive to the same symmetry case as of the nonmagnetic system, which can be described by the Z_2 invariant.

The parities of the Bloch's functions, with respect to the inversion symmetry operation (or equivalently a superposition of C_2 and fractional translation), were examined for the manifold of the entangled valence states—in a number of 70 bands per spinor—printed in Figure S4 in SI. The product (δ) of the parities (ξ_i) within this manifold is given in Table 1 for the Γ-point and the three TRIM points (TRIM = time-reversal invariant momentum): $X = (1/2, 0, 0)$, $Z = (0, 0, 1/2)$ and $M = (1/2, 0, 1/2)$. The parities of the two bands at the VBT and CBM are also included in Table 1. The list of the characters of the magnetic double point group $C_{2v}(2)$ is in Table S1 in SI. The irreducible representations assigned to the considered states are enclosed in SI in Tables S2–S5 for the ferromagnetic phase and Tables S6–S9 for the antiferromagnetic phase. In conclusion, both systems presented in this work are characterized by the Chern number [38] equal to 1.

The pressure evolution of the 2D band structures and the corresponding 1D edge states is presented for the FM phase in Fig. 4. The larger overlap of the p_z orbitals, with the applied pressure, causes three effects: (1) the bandgaps become smaller, (2) the local magnetic

Table 1 The product δ of the parities of the Bloch functions belonging to the manifold of the entangled valence bands at four high symmetry points, counted per large spinor component

Phase	ν	δ Γ	δ X	δ Z	δ M	$\xi^{VBT}_{(1,2)}/\xi^{CBM}_{(1,2)}$ Γ	$\xi^{VBT}_{(1,2)}/\xi^{CBM}_{(1,2)}$ X	$\xi^{VBT}_{(1,2)}/\xi^{CBM}_{(1,2)}$ Z	$\xi^{VBT}_{(1,2)}/\xi^{CBM}_{(1,2)}$ M
FM	1	1	− 1	1	1	(+,+)/(−,+)	(+,−)/(+,−)	(−,+)/(+,−)	(+,−)/(−,+)
AF	1	− 1	1	− 1	− 1	(−,+)/(−,+)	(+,+)/(+,−)	(+,+)/(−,+)	(−,+)/(+,+)

The parities of the two bands at VBT and CBM are denoted $\xi^{VBT}_{(1,2)}$ and $\xi^{CBM}_{(1,2)}$. The Z_2 invariant ν indicates the topological phase in 2D. It is given as a product of all δ's, which is $(-1)^{\nu} = \prod_i \delta_i$, where i runs over four corners of the Brillouin zone in 2D

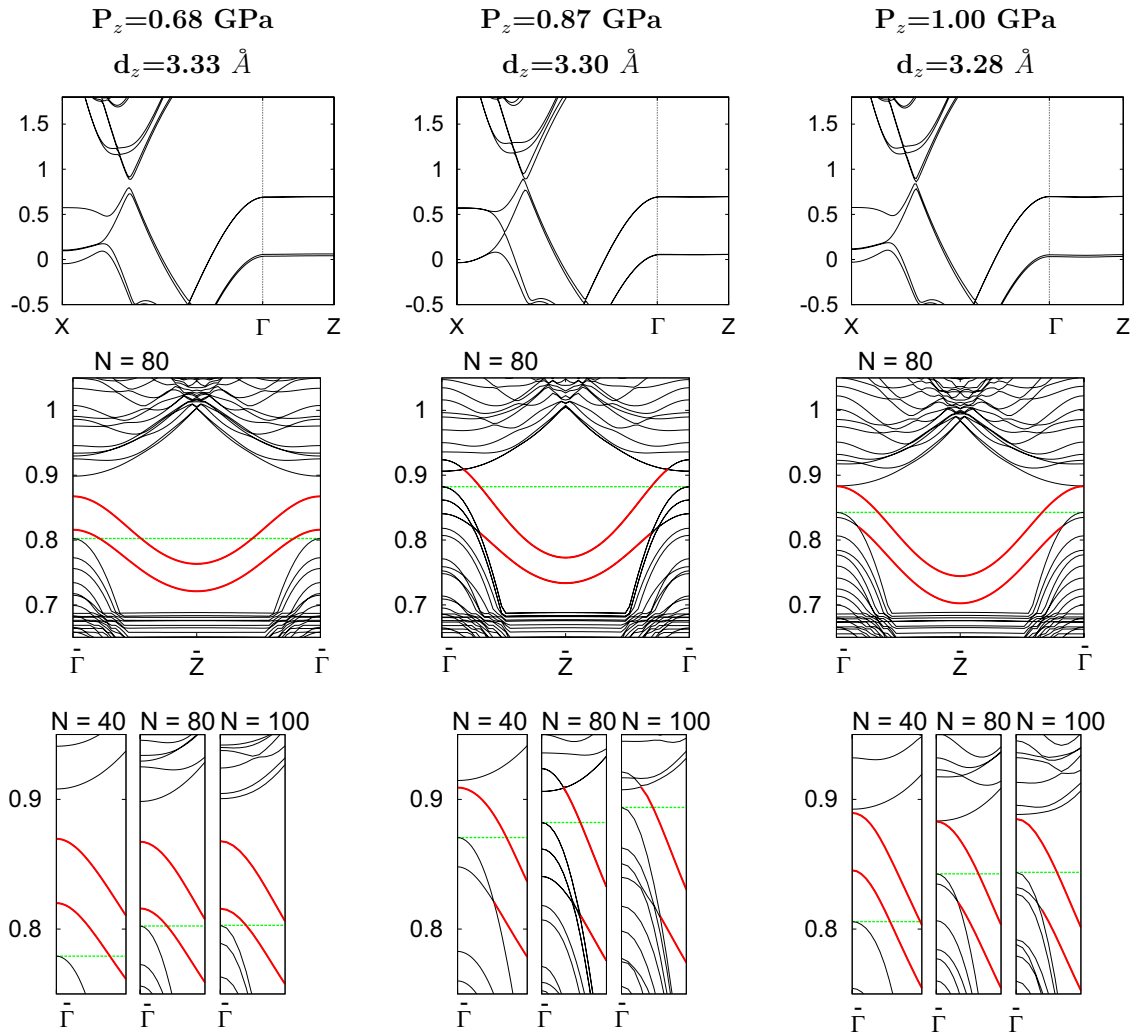

Fig. 4 The pressure evolution of the 2D band structure and the 1D truncated band structure, for the FM phase. The vertical distances d_z between the nanobelts, as well as the pressures, are given above the corresponding panels. The valence band maximum of the 1D truncated structure is marked with the green dashed line. The edge states are marked with red. The number of cells, N, in the truncated finite direction (X-axis) is given above the 1D structures. The last row presents enlarged regions close to the Γ-point. The energy scale is common for all three choices of N

moments at the nanobelt edges slightly increase, (3) the edge states in the 1D bandgap become gapless. As a consequence, around the pressure of c.a. 0.87 GPa, the edge states become gapless. The 1D dispersions depend slightly on the number of cells, N, in the truncated direction (X-axis). We present these details in Figs. 4 and S6 in SI, for $N = 40, 80, 100$. It is interesting that the edge

states move not monotonically with both the pressure and the thickness of the truncated structure.

The AF magnetic topological crystalline phase could be viewed as an example of the TCIs earlier predicted from the purely symmetrical considerations [31, 32]. The $\tau\Theta$ model [32] (with the glide mirror symmetry, as in our case) was discussed for a layered structure of the antiferromagnetically coupled planes, where the spins are perpendicular to the stacked planes. Such 3D structure was shown to possess the gapless edge states protected by the $\hat{\Pi}$ symmetry defined as a matrix of C_4 operations of two magnetic sublayers. In the AF phase studied here, this kind of stacking could be achieved on top of the 2D structures, if the belts are periodically repeated along the previously nonperiodic direction, i.e., the *Y*-axis. Building such 3D structure is plausible, due to the existence of the hydrogen bonds between the alternated O= and H-zigzag terminations.

3 Discussion

There is a quest for robust magnetic topological insulators for spintronic applications. The ways could be twofold: either to search over the intrinsically magnetic systems like Heusler compounds [18, 39], or via doping of the TIs with magnetic elements [19–28]. Doping of the TIs with the transition metals might lead to an opening of the gap in the topological surface states. But this is not a rule. It has been postulated that the magnetic anisotropy plays a role in that effect [27]. Namely, in 3D TIs, the out-of-surface magnetic polarization was believed to open the gap, as in the case of Mn-doped Bi_2Te_3. While the magnetic moments parallel to the surface were believed not to harm the surface states, as for the Co doping. With respect to the magnetic anisotropy, the doping at the surface or in the bulk usually makes a difference [27]. Recently, the above rule about the anisotropy and the gapless states has been contradicted, and the independence of the topological protection on magnetization was evidenced [28].

The 2D system presented in this work is intrinsically magnetic, with the magnetic moments localized at the plane spanned by the stacking axis and the zigzag edge of the belt. The belt has its thickness. In our case, it is sixteen carbons along the armchair chain of graphene, terminated with O and H. The belts are stacked with the AB-type reversed order. Such that each oxygen is located vertically between the carbons adjacent to the hydrogens of the belt below and belt above. This is important from the point of view of the magnetic interactions. The FM phase, with respect to the coupling between the belts in the stack, is energetically more favorable, by 31 meV, than the AF phase. The magnetic coupling occurs despite a quite large distance between the stacked layers, and the oxygen atoms are vertically separated by the two stacking distances, around 6.88 Å. However, the spin maps of the FM phase show the spin-density shifted from the belts plane close to the carbons adjacent to hydrogens. If we focus on the magnetic anisotropy, all O-centered moments are oriented out of the 2D surface. While the carbons along the armchair host much weaker magnetic moments than those of oxygens. The carbon moments are in the alternated spin order across the belt. This is a kind of a spin wave, schematically presented in Fig. 5a and in detail in Figure S5a in SI. After stacking the belts, the moments at the vertically overlapping carbons are parallel to each other. Therefore, weakly antiferromagnetic exchange across the belt

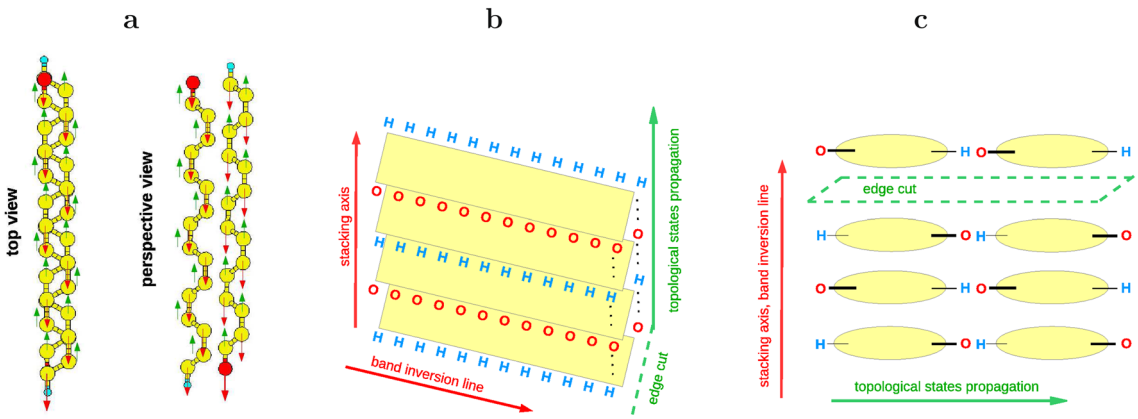

Fig. 5 The schematic view at: **a** the magnetic structure of the stacked nanobelts (the red and green arrows represent the positions of the local spins up and down), **b** the edge states propagation between the belts (the O···H-interaction direction, which is along the stacking *Z*-axis), **c** the edge states propagation in the 2D molecular crystal from Ref. [9] (also the O···H-interaction direction, which is one of the planar axes in this case)

drives the ferromagnetic exchange between the belts and also between the vertically coupled oxygens of every second belt. Moreover, the triangular symmetry of the system disfavors the AF order between the oxygens along the zigzag edge. If the AF order along the zigzag was existent, then the magnetic system would be frustrated, as shown in Figure S5b in SI. But it does not occur. The DFT calculations initialized at the AF-zigzag configuration converge to the spin unpolarized result, with the total energy higher than the FM phase, by 43 meV. The long-range ferromagnetic order in these belts might be robust even above the room temperature. This expectation is based on the similarities with the systems without the intentional O= and H– saturation [40–42].

The topological edge states form when one cuts through the belts, and not between the belts. Hence, the edge states propagate between the stacked layers. On the other hand, the local magnetic moments are parallel to the topological edge. Thus, the graphene belts would confirm an observation about the correlation between magnetic anisotropy and opening or not of the gap within the surface states [27]. This fact, however, is coincidental because our system should not be viewed as the TI material with the impurity states. This is a system where an intrinsic magnetism coexists with the crystal topological phase at a small pressure.

It is interesting to note that the propagation direction of the edge states along the stacking axis is parallel to the O···H-interaction direction. Whereas the bandgap location and the band inversion—although only partial—are between the states propagating along the belt axis. Similar situation was in the case of the 2D molecular crystal, namely in the π-stacked phenalene derivatives planarly interacting via the hydrogen bonds [9]. The edge states in that system also propagated along the O···H-interaction direction, whereas the bandgap and band inversion were between the states propagating along the stacking direction. The aforementioned systems and their topological directions are schematically drawn in Fig. 5b, c, for these and the earlier reported TCIs, respectively. It is remarkable, that the carriers at the topological states move between the weakly interacting parts of the system, and not through the covalent bonds, for both systems. Additionally, not the π-stacking axis, but the hydrogen bonds pin the propagation direction of the edge states in these numerically just-discovered TCIs.

From the symmetry-group point of view, the presented 2D systems are similar to the antiferromagnetic 3D TCIs constructed of the stacked 2D layers [31, 32], while the ferromagnetic case might be similar to the filling-enforced semimetals [33]. However, with the difference that the access to the edge states in our case is via the excitation of electrons, because the band gap is almost 1 eV above the Fermi level. Our systems are metallic when they are charge undoped.

In summary, the intrinsically magnetic, the FM and AF coupled, 2D TCIs are predicted under a small pressure in the AB-type π-stacked O= and H– terminated zigzag graphene nanobelts. The edge states dispersions are nondegenerate for the opposite spins. This is the second system just found [9] where the structures based on the benzene rings, π-stacking and O···H-interactions are characterized with the metallic edge states. These states become gapless under a small pressure applied along the stacking axis. It would be desirable to take these and other hydrogen-interacting systems under a magnifying glass and conduct the experimental investigations.

4 Methods

The density functional theory [43, 44] calculations were performed with the Quantum ESPRESSO (QE) package [45], which is based on the plane waves and the pseudopotentials for atomic cores. The norm-conserving pseudopotentials were used, and the energy cutoff of 60 Ry for the plane waves was set. The exchange-correlation functional was gradient corrected with the Perdew–Burke–Ernzerhof parametrization [46]. The uniform *k*-mesh by Monkhorst and Pack [47] with the 5-point grid along the stack and 10-point grid along the belt axis was sufficient to converge the band structure. The vacuum space of 20 Å was set between the 2D slabs in the nonperiodic direction. The geometry optimization was performed with the Broyden–Fletcher–Goldfarb–Shanno algorithm [48] until forces were smaller than 1 meV/Å.

For an accurate interpolation of the band structures, the wannier90 package [49] was used. It enables finding the maximally localized Wannier functions for the composite bands [50, 51]. The tight-binding model for the edge states analysis was constructed with the DFT Bloch functions. They were used for the generation of the Wannier functions [50]. Then, the Kohn-Sham Hamiltonian [43, 44] between these well-localized functions was built. In the tight-binding simulations with the pythTB code [52], the cutoff for the nonvanishing matrix elements was set to 0.005 eV. The parities of the Bloch functions at the TRIM points were obtained with the bands.x utility from the QE package.

Acknowledgements Thanks to Sinisa Coh and Maciej Czuchry for their help with pythTB. Calculations have been performed in the Cyfronet Computer Centre using Prometheus computer, which is a part of the PL-Grid Infrastructure.

Funding This study was funded by The National Science Centre of Poland (the Project No. DEC-2012/07/B/ST3/03412).

Compliance with ethical standards

Conflict of interest The authors declare that they have no conflict of interest.

References

1. Novoselov KS, Geim AK, Morozov SV, Jiang D, Zhang Y, Dubonos SV, Grigorieva IV, Firsov AA (2004) Electric field effect in atomically thin carbon films. Science 306:666
2. Castro Neto AH, Guinea F, Peres NMR, Novoselov KS, Geim AK (2009) The electronic properties of graphene. Rev Mod Phys 81:109162
3. Zhou J, Liang Q, Dong J (2010) Enhanced spin–orbit coupling in hydrogenated and fluorinated graphene. Carbon 48:1405
4. Balakrishnan J, Koon GKW, Jaiswal M, Castro Neto AH, Özyilmaz B (2013) Colossal enhancement of spin–orbit coupling in weakly hydrogenated graphene. Nat Phys 9:284
5. Kindermann M (2015) Topological crystalline insulator phase in graphene multilayers. Phys Rev Lett 114:226802
6. Yin L-J, Jiang H, Qiao J-B, He L (2016) Direct imaging of topological edge states at a bilayer graphene domain wall. Nat Commun 7:11760
7. Martin I, Blanter YM, Morpurgo AF (2008) Topological confinement in bilayer graphene. Phys Rev Lett 100:036804
8. Vaezi A, Liang Y, Ngai DH, Yang L, Kim E-A (2013) Topological edge states at a tilt boundary in gated multilayer graphene. Phys Rev X3:021018
9. Wierzbowska M (2017) Gapless edge states in (C, O, H)-built molecular system with π-stacking and hydrogen bonds. Sci Rep 7:9888
10. Hasan MZ, Kane CL (2010) Colloquium: topological insulators. Rev Mod Phys 82:3045
11. Fu L (2011) Topological crystalline insulators. Phys Rev Lett 106:106802
12. Chong YD, Wen X-G, Soljacic M (2008) Effective theory of quadratic degeneracies. Phys Rev B 77:235125
13. Yu J-X, Che JG (2016) An anomalous band inversion protected by symmetry in a topological insulator of the Kane–Mele model. Phys Rev B 93:035449
14. Fujita M, Wakabayashi K, Nakada K, Kusakabe K (1996) Peculiar localized state at zigzag graphite edge. J Phys Soc Jpn 65:1920
15. Son YW, Cohen ML, Louie SG (2006) Half-metallic graphene nanoribbons. Nature 444:347
16. Wierzbowska M (2016) New memory devices based on the proton transfer process. Nanotechnology 27:015202
17. Verzhbitskiy IA, De Corato M, Ruini A, Molinari E, Narita A, Hu Y, Schwab MG, Bruna M, Yoon D, Milana S, Feng X, Müllen K et al (2016) Raman fingerprints of atomically precise graphene nanoribbons. Nano Lett 16:3442
18. Múller RA, Lee-Hone NR, Lapointe L, Ryan DH, Pereg-Barnea T, Bianchi AD, Mozharivskyj Y, Flacau R (2014) Magnetic structure of *GdBiPt*: a candidate antiferromagnetic topological insulator. Phys Rev B 90:041109(R)
19. Sessi P, Biswas RR, Bathon T, Storz O, Wilfert S, Barla A, Kokh KA, Tereshchenko OE, Fauth K, Bode M, Balatsky AV (2016) Dual nature of magnetic dopants and competing trends in topological insulators. Nat Commun 7:12027
20. Ye M, Li W, Zhu S, Takeda Y, Saitoh Y, Wang J, Pan H, Nurmamat M, Sumida K, Ji F, Liu Z, Yang H et al (2015) Carrier-mediated ferromagnetism in the magnetic topological insulator Cr-doped $(Sb, Bi)_2 Te_3$. Nat Commun 6:8913
21. Liu C-X, Qi X-L, Dai X, Fang Z, Zhang S-C (2008) Quantum anomalous Hall effect in $Hg_{1-y} Mn_y Te$ quantum wells. Phys Rev Lett 101:146802
22. Wray LA, Xu S-Y, Xia Y, Hsieh D, Fedorov AV, Lin H, Bansil A, Hor YS, Cava RJ, Hasan MZ (2011) A topological insulator surface under strong Coulomb, magnetic and disorder perturbations. Nat Phys 7:32
23. Chen YL, Chu JH, Analytis JG, Liu ZK, Igarashi K, Kuo HH, Qi XL, Mo SK, Moore RG, Lu DH, Hashimoto M, Sasagawa T et al (2010) Massive Dirac fermion on the surface of a magnetically doped topological insulator. Science 329:659
24. Scholz MR, Sánchez-Barriga J, Marchenko D, Varykhalov A, Volykhov A, Yashina LV, Rader O (2012) Tolerance of topological surface states towards magnetic moments: Fe on $Bi_2 Se_3$. Phys Rev Lett 108:256810
25. Valla T, Pan Z-H, Gardner D, Lee YS, Chu S (2012) Photoemission spectroscopy of magnetic and nonmagnetic impurities on the surface of the $Bi_2 Se_3$ topological insulator. Phys Rev Lett 108:117601
26. Scholz MR, Sánchez-Barriga J, Marchenko D, Varykhalov A, Volykhov A, Yashina LV, Rader O (2013) Intact dirac cone of $Bi_2 Te_3$ covered with a monolayer Fe. Phys Status Solidi RRL 7:139
27. Sessi P, Reis F, Bathon T, Kokh KA, Tereshchenko OE, Bode M (2014) Signatures of Dirac fermion-mediated magnetic order. Nat Commun 5:5349
28. Sánchez-Barriga J, Varykhalov A, Springholz G, Steiner H, Kirchschlager R, Bauer G, Caha O, Schierle E, Weschke E, Ünal AA, Valencia S, Dunst M et al (2016) Nonmagnetic band gap at the Dirac point of the magnetic topological insulator $(Bi_{1-x} Mn_x)_2 Se_3$. Nat Commun 7:10559
29. Lu J, Shan W-Y, Lu H-Z, Shen S-Q (2011) Non-magnetic impurities and in-gap bound states in topological insulators. New J Phys 13:103016
30. Peng X, Yang Y, Singh RRP, Savrasov SY, Yu D (2016) Spin generation via bulk spin current in three-dimensional topological insulators. Nat Commun 7:10878
31. Fang C, Gilbert MJ, Bernevig BA (2013) Topological insulators with commensurate antiferromagnetism. Phys Rev B 88:085406
32. Zhang R-X, Liu C-X (2015) Topological magnetic crystalline insulators and corepresentation theory. Phys Rev B 91:115317
33. Watanabe H, Po HC, Vishwanath A (2017) Structure and topology of band structures in the 1651 magnetic space groups. arXiv :1707.01903
34. Wawrzyniak-Adamczewska M, Wierzbowska M (2016) Separate-path electron and hole transport across π-stacked ferroelectrics for photovoltaic applications. J Phys Chem C 120:7748
35. Wehrenfennig C, Eperon GE, Johnston MB, Snaith HJ, Herz LM (2014) High charge carrier mobilities and lifetimes in organolead trihalide perovskites. Adv Mater 26:1584
36. Wehrenfennig C, Liu M, Snaith HJ, Johnston MB, Herz LM (2014) Charge-carrier dynamics in vapour-deposited films of the organolead halide perovskite $CH_3 NH_3 PbI_{3-x} Cl_x$. Energy Environ Sci 7:2269
37. Calik M, Auras F, Salonen LM, Bader K, Grill I, Handloser DD, Medina DD, Dogru M, Lübermann F, Trauner D, Hartschuh A, Bein T (2014) Extraction of photogenerated electrons and holes

from a covalent organic framework integrated heterojunction. J Am Chem Soc 136:17802
38. Fu L, Kane CL (2007) Topological insulators with inversion symmetry. Phys Rev B 76:045302
39. Felser C, Wollmann L, Chadov S, Fecher GH, Parkin SSP (2015) Basics and prospective of magnetic Heusler compounds. Appl Phys Lett Mater 3:041518
40. Joly VLJ, Kiguchi M, Hao S-J, Takai K, Enoki T, Sumii R, Amemiya K, Muramatsu H, Hayashi T, Kim YA, Endo M, Campos-Delgado J et al (2010) Observation of magnetic edge state in graphene nanoribbons. Phys Rev B 81:245428
41. Magda GZ, Xiaozhan J, Hagymasi I, Vancso P, Osvath Z, Nemes-Incze P, Hwang C, Biro LP, Tapaszto L (2014) Room-temperature magnetic order on zigzag edges of narrow graphene nanoribbons. Nature 514:608
42. Makarova TL, Shelankov AL, Zyrianova AA, Veinger AI, Tisnek TV, Lähderanta E, Shames AI, Okotrub AV, Bulusheva LG, Chekhova GN, Pinakov DV, Asanov IP et al (2015) Edge state magnetism in zigzag-interfaced graphene via spin susceptibility measurements. Sci Rep 5:13382 1
43. Hohenberg P, Kohn W (1964) Inhomogeneous electron gas. Phys Rev 136:B864
44. Kohn W, Sham LJ (1965) Self-consistent equations including exchange and correlation effects. Phys Rev 140:A1133
45. Giannozzi P, Baroni S, Bonini N, Calandra M, Car R, Cavazzoni C, Ceresoli D, Chiarotti GL, Cococcioni M, Dabo I et al (2009) QUANTUM ESPRESSO: a modular and open-source software project for quantum simulations of materials. J Phys Condens Matter 21(39):395502
46. Perdew JP, Burke K, Ernzerhof M (1996) Generalized gradient approximation made simple. Phys Rev Lett 77(18):3865
47. Monkhorst HJ, Pack JD (1976) Special points for Brillouin-zone integrations. Phys Rev B 13(12):5188
48. Fletcher R (1987) Practical methods of optimization, 2nd edn. Wiley, Chichester
49. Mostofi AA, Yates YR, Lee YS, Souza I, Vanderbilt D, Marzari N (2008) wannier90: a tool for obtaining maximally localised Wannier functions. Comput Phys Commun 178:685
50. Marzari N, Vanderbilt D (1997) Maximally localized generalized Wannier functions for composite energy bands. Phys Rev B 56:12847
51. Marzari N, Mostofi AA, Yates JR, Souza I, Vanderbilt D (2012) Maximally localized Wannier functions: theory and applications. Rev Mod Phys 84:1419
52. Coh S, Vanderbilt D (2018) Python tight binding (PythTB) code. http://www.physics.rutgers.edu/pythtb/index.html